Journal of Sound and Vibration, 331(4), pp. 833-848, doi: 10.1016/j.jsv.2011.09.023

INTERACTION OF A NON-SELF-ADJOINT ONE-DIMENSIONAL CONTINUUM AND MOVING MULTI-DEGREE-OF-FREEDOM OSCILLATOR

Piotr Omenzetter

Department of Civil and Environmental Engineering
The University of Auckland
Private Bag 92019
Auckland Mail Centre
1142 Auckland
New Zealand

Tel. 64-9-923-8138
Fax: 64-9-373-7462
E-mail: p.omenzetter@auckland.ac.nz

ABSTRACT

A method for computing the dynamic responses due to the interaction of two non-self-adjoint systems: a linear, one-dimensional (1D) continuum and a linear, multi-degree-of-freedom (MDOF) oscillator travelling over the continuum, is presented. The solution method is applicable to a broad class of 1D continua, whose dynamics may be governed by various linear operators and subjected to different boundary conditions. The problem is reduced to the integration of a system of linear differential equations with time dependent coefficients. These coefficients are found to depend on eigenvalues as well as eigenfunctions and eigenvectors of the continuum and the oscillator. Two examples are included, representing bridge and railway track vibrations, to demonstrate the application of the method and discuss its convergence.

Keywords: vehicle-bridge interaction, moving oscillator, non-self-adjoint operator, bridge vibrations, railway track vibrations

1. INTRODUCTION

The dynamic response of flexible structures due to moving loads is an important issue in engineering. The problem is relevant in vehicle dynamics, studies of band and circular saw blades, machine chain and belt drives, computer hard drives and many other applications. Among civil engineering applications are analyses of dynamic response of railway, roadway and pedestrian bridges due to traffic loads, and studies of roadway pavements, railroad tracks, airport runways, cable railways, floors etc. A large amount of analytical research has been devoted to the topic, e.g., [1]-[9]. In early studies, vehicle loads were represented as moving constant or time-varying forces, a moving mass, or a moving sprung mass. Later, more sophisticated multi-degree-of-freedom (MDOF) models were proposed, and the various linear as well as non-linear stiffness and damping characteristics of vehicles were considered. The development of fast computers also facilitated a much more detailed modelling of bridges and other structures through the use of Finite Element Method (FEM). From the point of view of computational effort, the modal based techniques are especially attractive. In the modal analysis process, one can naturally truncate the number of modes and thus prevent excessive computational burden, whereas FEM based modelling may lead to a large computational load, especially when two or three-dimensional structural models need to be analyzed. Such methods are also useful as a tool for checking and evaluating FEM solutions. However, most of the studies using the modal approach have developed ad hoc solutions valid only for particular types of structural and vehicle models considered. Little analytical work is available on the development of a general modal expansion technique capable of resolving the interaction problem for a broader class of models.

Pesterev and Bergman [10] considered the problem of the vibrations of a general category of linear, conservative, one-dimensional (1D) continua carrying a moving, linear,

conservative, one-degree-of-freedom (1DOF) oscillator. They established the solution of the interaction problem in the form of a series in terms of the eigenfunctions of the isolated continuum. The time dependent factors of the expansion were demonstrated to obey a system of linear differential equations with time dependent coefficients. These coefficients turned out to depend on natural frequencies and eigenfunctions of the isolated continuum, mass of the oscillator, and stiffness of the interaction spring. This method can be used to examine any 1D linear conservative continuum, regardless of the governing equation of motion or boundary conditions. Later, the authors expanded their method ([11]), which enabled the investigation of the interaction problem for non-conservative, non-self-adjoint continua as well. However, these derivations were limited to the conservative vehicle-structure interaction forces and 1DOF vehicle model, making the obtained method only of limited usefulness in practical application to design and analysis. Omenzetter and Fujino ([12]) extended the work of Pesterev and Bergman and obtained solutions for a moving MDOF oscillator, where both the continuum and the oscillator were assumed to be self-adjoint, classically damped systems. Their solution employed modal decomposition for both the continuum and the oscillator, which was a unique approach compared to the existing previous studies.

The novel contribution of the present study is the consideration of a non-self-adjoint continuum and a non-self-adjoint MDOF vehicle model, interacting with the continuum at several contact points through linear elastic and viscous forces. The solution of the structure-vehicle interaction problem is obtained in terms of a modal expansion using eigenfunctions and eigenvectors of the isolated continuum and oscillator, respectively. The primary challenge was that for non-self-adjoint operators the direct and adjoint eigenvalue problems yield different sets of eigenfunctions or eigenvectors and these are furthermore complex valued. The problem of computing the time dependent terms of the modal expansion is reduced to the

integration of a system of linear differential equations with time dependent real coefficients. The coefficients of these equations are derived in terms of the complex eigenvalues as well as eigenfunctions and eigenvectors of the isolated continuum and the MDOF oscillator, and stiffness and damping of the interaction elements. The obtained analytical method is applied to two numerical examples, i.e., bridge and railway track vibrations, which demonstrate its use and study convergence.

2. THEORY

2.1. Problem Formulation

In a study of the vehicle-structure interaction, two equations of motion can be written for the isolated continuum and the isolated moving oscillator, respectively. These equations are coupled due to the presence of interaction forces at the contact points. A 1D continuous system and a MDOF oscillator moving over it are shown Fig. 1. The part of the system that is, for illustrative purposes, confined within dashed boundaries and consists of those masses, springs and dashpots that are not in a direct contact with the continuum is referred to as the vehicle model or oscillator. Those springs and dashpots that are in a direct contact with the continuum are referred to as the interaction elements. The locations on the continuum are described by variable x, and the continuum occupies the interval $0 \le x \le L$, where L is the length of the continuum. The lateral deflections of the continuum at location x and time t are described by a function $u_c(x,t)$, while $u_c(x,0)$ and $\dot{u}_c(x,0)$ are initial displacements and velocities, respectively. Distributed external forces acting on the continuum are denoted by $f_c(x,t)$. The displacements of the vehicle under the action of external forces, $f_v(t)$, are denoted by a vector $u_v(t)$, while $u_v(0)$ and $\dot{u}_v(0)$ are initial conditions. (Note that the

mathematical formulations presented herein treat both differential operators/matrices and functions/vectors in the same way as operators and objects in their respective vector spaces. To emphasize this, the more traditional notational convention of using bold characters for matrices and vectors has been dispensed with.) The derivation of a continuum-vehicle interaction governing equation of motion was described in detail in [12]; in this paper, a shortened form of problem formulation is given. The equation of motion can be succinctly expressed in the following form ([12]):

$$\left(\hat{A}+\hat{\Theta}^{*}\hat{L}\hat{\Theta}\right)u=F+P \tag{1}$$

where the symbols introduced in Eq. (1) are as follows:

$$\hat{A}=\begin{bmatrix}\hat{A}_c & 0\\ 0 & \hat{A}_v\end{bmatrix},\ \hat{\Theta}=\begin{bmatrix}\hat{\Pi}_x\left[x_{cv}(t)\right] & -T\end{bmatrix},\ \hat{\Theta}^{*}=\begin{bmatrix}\hat{\Delta}_x\left[x_{cv}(t)\right]\\ -T^{T}\end{bmatrix},\ \hat{L}=K_{cv}+C_{cv}\frac{d}{dt} \tag{2a-d}$$

$$u=\begin{bmatrix}u_c(x,t) & u_v^{T}(t)\end{bmatrix}^{T},\ F=\begin{bmatrix}f_c(x,t) & f_v^{T}(t)\end{bmatrix}^{T},\ P=\begin{bmatrix}P_c(x,t) & P_v^{T}(t)\end{bmatrix}^{T} \tag{2e-g}$$

The asterisk denotes an adjoint operator, and superscript "T" a transposition of a vector or matrix. Operators $\hat{A}_c$ and $\hat{A}_v$ govern the motion of the isolated continuum and oscillator, respectively, and can be written as follows:

$$\hat{A}_c u_c(x,t)=\hat{M}_c\frac{\partial^2 u_c(x,t)}{\partial t^2}+\hat{C}_c\frac{\partial u_c(x,t)}{\partial t}+\hat{K}_c u_c(x,t) \tag{3a}$$

$$\hat{A}_v u_v(t)=M_v\frac{d^2 u_v(t)}{dt^2}+C_v\frac{du_v(t)}{dt}+K_v u_v(t) \tag{3b}$$

$\hat{M}_c$, $\hat{C}_c$ and $\hat{K}_c$ are spatial linear differential operators, whereas M_v, C_v and K_v are square matrices. Operators $\hat{M}_c$ and M_v are positive definite. Operators $\hat{C}_c$ and C_v describe the effects of damping and gyroscopic forces, while $\hat{K}_c$ and K_v these of stiffness and circulatory

forces. Operators $\hat{\Theta}$, $\hat{\Theta}^*$ and $\hat{L}$ describe the coupling between the continuum and oscillator. Operators $\hat{\Theta}$ and its adjoint $\hat{\Theta}^*$ consist of the sensor operator, $\hat{\Pi}_x[x_{cv}(t)]$, and the effector operator, $\hat{\Delta}_x[x_{cv}(t)]$, as well as matrix T that transforms the displacements of the oscillator into the displacements resulting in interaction forces. The sensor and effector operators form an adjoint operator pair and have the following forms ([13]):

$$\hat{\Pi}_x[x_{cv}(t)] = \left[\hat{\pi}_x[x_{cv,1}(t)] \quad \ldots \quad \hat{\pi}_x[x_{cv,N_{cv}}(t)]\right]^T \tag{4a}$$

$$\hat{\Delta}_x[x_{cv}(t)] = \hat{\Pi}_x^*[x_{cv}(t)] = \left[\delta[x - x_{cv,1}(t)] \quad \ldots \quad \delta[x - x_{cv,N_{cv}}(t)]\right] \tag{4b}$$

where $\hat{\pi}_x(x_0)$ is an assignment operator acting on a function $z(x)$ as follows:

$$\hat{\pi}_x(x_0)z(x) = z(x_0) \tag{5}$$

and δ denotes the Dirac delta function. In Eq. (4), $x_{cv}(t)$ is the vector of contact point locations of size N_{cv}. Operator $\hat{L}$ defined in Eq. (2d) accounts for the stiffness and damping of the interaction elements, where K_{cv} and C_{cv} are their stiffness and damping matrices, respectively.

Vector P describes the inputs to the coupled system due to the initial conditions and can be found as

$$P = \hat{M}\delta(t)\dot{u}(x,0) + \hat{M}\dot{\delta}(t)u(x,0) + \left\{\hat{C} + \Theta^*\left[x_{cv}(0)\right]C_{cv}\Theta\left[x_{cv}(0)\right]\right\}\left[\delta(t)u(x,0)\right] \tag{6}$$

where

$$\hat{M} = \begin{bmatrix} \hat{M}_c & 0 \\ 0 & \hat{M}_v \end{bmatrix}, \; \hat{C} = \begin{bmatrix} \hat{C}_c & 0 \\ 0 & C_v \end{bmatrix} \tag{7a, b}$$

2.2. Eigenvalue Problems

This study attempts to establish a solution for the interaction problem in the form of a modal expansion using eigenvalues as well as eigenfunctions of the continuum and eigenvectors of the oscillator. Therefore, to lay the ground for subsequent derivations in this section the eigenvalue problems are formulated and the properties of the eigenfunctions and eigenvectors important for this study are discussed.

The direct and adjoint eigenvalue problems associated with the equation of motion of the isolated continuum can be written as follows:

$$\left(\lambda_{c,k}^2 \hat{M}_c + \lambda_{c,k} \hat{C}_c + \hat{K}_c\right)\phi_{c,k}(x) = 0\,,\ k = \pm 1, \pm 2, \ldots \tag{8a}$$

$$\left(\overline{\lambda}_{c,k}^2 \hat{M}_c + \overline{\lambda}_{c,k} \hat{C}_c^* + \hat{K}_c^*\right)\psi_{c,k}(x) = 0\,,\ k = \pm 1, \pm 2, \ldots \tag{8b}$$

where the overbar denotes complex conjugation, $\lambda_{c,k}$ is the k-th eigenvalue, and $\phi_{c,k}(x)$ and $\psi_{c,k}(x)$ are eigenfunctions of the direct and adjoint eigenvalue problem, respectively. It is useful to extend the domain over which the eigenfunctions are defined to all real numbers, $-\infty < x < +\infty$, by assigning to the eigenfunctions values of zero outside the interval $0 \le x \le L$. Having done so, all the formulas are the same irrespective of the current location of the oscillator ([12]). The eigenvalues and eigenvectors possess the following properties: $\lambda_{c,-k} = \overline{\lambda}_{c,k}$, $\phi_{c,-k}(x) = \overline{\phi}_{c,k}(x)$ and $\psi_{c,-k}(x) = \overline{\psi}_{c,k}(x)$. In general, the eigenvectors are complex and nonorthogonal, however, the following normalization condition ([14]) for $\phi_{c,k}(x)$ and $\psi_{c,k}(x)$ holds:

$$\int_0^L \overline{\psi}_{c,k}(x)\hat{M}_c\phi_{c,k}(x)\,\mathrm{d}x - \frac{1}{\lambda_{c,k}^2}\int_0^L \overline{\psi}_{c,k}(x)\hat{K}_c\phi_{c,k}(x)\,\mathrm{d}x = 2 \tag{9}$$

Likewise, the direct and adjoint eigenvalue problems associated with the equation of motion of the isolated vehicle are:

$$\left(\lambda_{v,k}^2 M_v + \lambda_{v,k} C_v + K_v\right)\phi_{v,k} = 0 \tag{10a}$$

$$\left(\overline{\lambda}_{v,k}^2 M_v + \overline{\lambda}_{v,k} C_v^T + K_v^T\right)\psi_{v,k} = 0 \tag{10b}$$

Among the eigenvalues which satisfy Eq. (10), there are non-zero-valued ones corresponding to vibratory modes and denoted by $\lambda_{vv,k}$ ($k = \pm 1, \pm 2, \ldots, \pm N_{vv}$), as well as zero-valued ones corresponding to rigid body modes and denoted by $\lambda_{vr,k}$ ($k = 1, 2, \ldots, N_{vr}$). The corresponding eigenvectors are $\phi_{vv,k}$ and $\psi_{vv,k}$, and $\phi_{vr,k}$ and $\psi_{vr,k}$. The conjugate properties of the eigenvalues and eigenvectors of the generally complex vibratory modes are the same as those of the continuum modes, i.e., $\lambda_{vv,-k} = \overline{\lambda}_{vv,k}$, $\phi_{vv,-k} = \overline{\phi}_{vv,k}$ and $\psi_{vv,-k} = \overline{\psi}_{vv,k}$; whereas the eigenvectors of the rigid body modes are all real. The eigenvector normalization condition takes the following forms:

$$\overline{\psi}_{vv,k}^T M_v \phi_{vv,k} - \frac{1}{\lambda_{vv,k}^2}\overline{\psi}_{vv,k}^T K_v \phi_{vv,k} = 2 \tag{11a}$$

for the vibratory modes, and

$$\psi_{vr,k}^T M_v \phi_{vr,k} = 1 \tag{11b}$$

for the rigid body modes, respectively.

2.3. Solution by Reduction to Ordinary Differential Equations

The solution of the interaction problem [Eq. (1)] is given by the following formula:

$$u = \left(\hat{A} + \hat{\Theta}^* \hat{L} \hat{\Theta}\right)^{-1}\left(F + P\right) \tag{12}$$

The inverse operator appearing in Eq. (12) can be found as ([15]):

$$\left(\hat{A}+\hat{\Theta}^{*}\hat{L}\hat{\Theta}\right)^{-1}=\hat{A}^{-1}-\hat{A}^{-1}\hat{\Theta}^{*}\hat{\chi}^{-1}\hat{L}\hat{\Theta}\hat{A}^{-1} \tag{13}$$

where the characteristic operator, $\hat{\chi}$, is given as

$$\hat{\chi}=\hat{I}+\hat{L}\hat{\Theta}\hat{A}^{-1}\hat{\Theta}^{*} \tag{14}$$

The inverse of operator $\hat{A}$ describing the vibrations of the isolated subsystems is:

$$\hat{A}^{-1}=\begin{bmatrix}\hat{A}_{c}^{-1} & 0\\ 0 & \hat{A}_{v}^{-1}\end{bmatrix} \tag{15}$$

To evaluate the operators $\hat{A}_{c}^{-1}$ and $\hat{A}_{v}^{-1}$, a modal expansion of the Green function ([14]) can be used, leading to the following formulas:

$$\hat{A}_{c}^{-1}=\int_{0}^{t}\int_{-\infty}^{\infty}\frac{1}{2}\sum_{k=\pm1}^{\pm\infty}\frac{1}{\lambda_{c,k}}e^{\lambda_{c,k}(t-\tau)}\phi_{c,k}(x)\bar{\psi}_{c,k}(\xi)\,f_{c}(\xi,\tau)\,\mathrm{d}\xi\,\mathrm{d}\tau \tag{16a}$$

$$\hat{A}_{v}^{-1}=\int_{0}^{t}\frac{1}{2}\sum_{k=\pm1}^{\pm N_{vv}}\frac{1}{\lambda_{vv,k}}e^{\lambda_{vv,k}(t-\tau)}\phi_{vv,k}\bar{\psi}_{vv,k}^{T}\,f_{v}(\tau)\,\mathrm{d}\tau+\int_{0}^{t}\sum_{k=1}^{N_{vr}}(t-\tau)\phi_{vr,k}\psi_{vr,k}^{T}\,f_{v}(\tau)\mathrm{d}\tau \tag{16b}$$

Introduce the notation for the following modal quantities: the modal external forces

$$Q_{c,k}(t)=\int_{-\infty}^{\infty}\bar{\psi}_{c,k}(x)\,f_{c}(x,t)\,\mathrm{d}x,\ k=\pm1,\pm2,\ldots \tag{17a}$$

$$Q_{vv,k}(t)=\bar{\psi}_{vv,k}^{T}\,f_{v}(t),\ k=\pm1,\pm2,\ldots,\pm N_{vv} \tag{17b}$$

$$Q_{vr,k}(t)=\psi_{vr,k}^{T}\,f_{v}(t),\ k=1,2,\ldots,N_{vr} \tag{17c}$$

the modal initial displacements and velocities

$$q_{c0,k}=-\frac{1}{\lambda_{c,k}^{2}}\int_{-\infty}^{\infty}\bar{\psi}_{c,k}(x)\hat{K}_{c}u_{c}(x,0)\,\mathrm{d}x,\ \dot{q}_{c0,k}=\int_{-\infty}^{\infty}\bar{\psi}_{c,k}(x)\hat{M}_{c}\dot{u}_{c}(x,0)\,\mathrm{d}x,\ k=\pm1,\pm2,\ldots \tag{18a, b}$$

$$q_{vv0,k}=-\frac{1}{\lambda_{vv,k}^{2}}\bar{\psi}_{vv,k}^{T}K_{v}u_{v}(0),\ \dot{q}_{vv0,k}=\bar{\psi}_{vv,k}^{T}(x)M_{v}\dot{u}_{c}(0),\ k=\pm1,\pm2,\ldots,\pm N_{vv} \tag{18c, d}$$

$$q_{vr0,\,k} = \psi_{vr,\,k}^{T} M_v u_v(0),\ \dot{q}_{vr0,\,k} = \psi_{vr,\,k}^{T}(x) M_v \dot{u}_c(0),\ k = 1, 2, \ldots, N_{vr} \tag{18e, f}$$

and the modal inputs due to the initial conditions

$$R_{c,k}(t) = \lambda_{c,k}\left\{\left(\frac{1}{\lambda_{c,k}}\dot{q}_{c0,k} + q_{c0,k}\right) + \frac{\left\{\Pi_x\left[x_{cv}(0)\right]\bar{\psi}_{c,\,k}(x)\right\}^{T} C_{cv}}{\lambda_{c,k}}\left[\frac{1}{2}\sum_{j=\pm 1}^{\pm\infty}\Pi_x\left[x_{cv}(0)\right]\phi_{c,\,j}(x)\left(\frac{1}{\lambda_{c,\,j}}\dot{q}_{c0,\,j} + q_{c0,\,j}\right)\right.\right.$$
$$\left.\left. -\frac{1}{2}\sum_{j=\pm 1}^{\pm N_{vv}} T\phi_{vv,\,j}\left(\frac{1}{\lambda_{vv,\,j}}\dot{q}_{vv0,\,j} + q_{vv0,\,j}\right) - \sum_{j=1}^{N_{vr}} T\phi_{vr,\,j} q_{vr0,\,j}\right]\right\}\delta(t), \quad k = \pm 1, \pm 2, \ldots \tag{19a}$$

$$R_{vv,k}(t) = \lambda_{vv,k}\left\{\left(\frac{1}{\lambda_{vv,k}}\dot{q}_{vv0,k} + q_{vv0,k}\right) + \frac{\bar{\psi}_{vv,\,k}^{T} T^{T} C_{cv}}{\lambda_{vv,k}}\left[\frac{1}{2}\sum_{j=\pm 1}^{\pm\infty}\Pi_x\left[x_{cv}(0)\right]\phi_{c,\,j}(x)\left(\frac{1}{\lambda_{c,\,j}}\dot{q}_{c0,\,j} + q_{c0,\,j}\right)\right.\right.$$
$$\left.\left. -\frac{1}{2}\sum_{j=\pm 1}^{\pm N_{vv}} T\phi_{vv,\,j}\left(\frac{1}{\lambda_{vv,\,j}}\dot{q}_{vv0,\,j} + q_{vv0,\,j}\right) - \sum_{j=1}^{N_{vr}} T\phi_{vr,\,j} q_{vr0,\,j}\right]\right\}\delta(t), \quad k = \pm 1, \pm 2, \ldots, \pm N_{vv} \tag{19b}$$

$$R_{vr,k}(t) = q_{vr0,k}\dot{\delta}(t) + \left\{\dot{q}_{vr0,k} + \bar{\psi}_{vr,\,k}^{T} T^{T} C_{cv}\left[\frac{1}{2}\sum_{j=\pm 1}^{\pm\infty}\Pi_x\left[x_{cv}(0)\right]\phi_{c,\,j}(x)\left(\frac{1}{\lambda_{c,\,j}}\dot{q}_{c0,\,j} + q_{c0,\,j}\right)\right.\right.$$
$$\left.\left. -\frac{1}{2}\sum_{j=\pm 1}^{\pm N_{vv}} T\phi_{vv,\,j}\left(\frac{1}{\lambda_{vv,\,j}}\dot{q}_{vv0,\,j} + q_{vv0,\,j}\right) - \sum_{j=1}^{N_{vr}} T\phi_{vr,\,j} q_{vr0,\,j}\right]\right\}\delta(t), \quad k = 1, 2, \ldots, N_{vr} \tag{19c}$$

Introduce the notation

$$\hat{\chi}^{-1}\hat{L}\hat{\Theta}\hat{A}^{-1}(F + P) = y(t) \tag{20}$$

Function $-y(t)$ can be recognized as the vector of interaction forces acting upon the continuum at the contact points with the oscillator ([12]). The modal interaction forces can now be defined as

$$Y_{c,k}(t) = -\left\{\Pi_x\left[x_{cv}(t)\right]\bar{\psi}_{c,\,k}(x)\right\}^{T} y(t),\ k = \pm 1, \pm 2, \ldots \tag{21a}$$

$$Y_{vv,\,k}(t) = \bar{\psi}_{vv,k}^{T} T^{T} y(t),\ k = \pm 1, \pm 2, \ldots, \pm N_{vv} \tag{21b}$$

$$Y_{vr,k}(t)=\psi_{vr,k}^{T}T^{T}y(t),\ k=1,2,\ldots,N_{vr} \tag{21c}$$

New variables, or modal coordinates, are defined as

$$q_{c,k}(t)=\int_0^t\frac{1}{\lambda_{c,k}}e^{\lambda_{c,k}(t-\tau)}\left[Q_{c,k}(\tau)+R_{c,k}(\tau)+Y_{c,k}(\tau)\right]\mathrm{d}\tau,\ k=\pm1,\pm2,\ldots \tag{22a}$$

$$q_{vv,k}(t)=\int_0^t\frac{1}{\lambda_{vv,k}}e^{\lambda_{vv,k}(t-\tau)}\left[Q_{vv,k}(\tau)+R_{vv,k}(\tau)+Y_{vv,k}(\tau)\right]\mathrm{d}\tau,\ k=\pm1,\pm2,\ldots,\pm N_{vv} \tag{22b}$$

$$q_{vr,k}(t)=\int_0^t(t-\tau)\left[Q_{vr,k}(\tau)+R_{vr,k}(\tau)+Y_{vr,k}(\tau)\right]\mathrm{d}\tau,\ k=1,2,\ldots,N_{vr} \tag{22c}$$

Differentiating Eqs. (22a, b) with respect to t once and Eq. (22c) twice, one obtains the following first or second order differential equations, respectively, satisfied by the modal coordinates:

$$\dot{q}_{c,k}(t)-\lambda_{c,k}q_{c,k}(t)=\frac{Q_{c,k}(t)+R_{c,k}(t)+Y_{c,k}(t)}{\lambda_{c,k}},\ k=\pm1,\pm2,\ldots \tag{23a}$$

$$\dot{q}_{vv,k}(t)-\lambda_{vv,k}q_{vv,k}(t)=\frac{Q_{vv,k}(t)+R_{vv,k}(t)+Y_{vv,k}(t)}{\lambda_{vv,k}},\ k=\pm1,\pm2,\ldots,\pm N_{vv} \tag{23b}$$

$$\ddot{q}_{vr,k}(t)=Q_{vr,k}(t)+R_{vr,k}(t)+Y_{vr,k}(t),\ k=1,2,\ldots,N_{vr} \tag{23c}$$

Expanding Eq. (20) and using the modal coordinates yields the formula for the interaction forces:

$$\begin{aligned}y(t)=&K_{cv}\left\{\frac{1}{2}\sum_{k=\pm1}^{\pm\infty}\Pi_x\left[x_{cv}(t)\right]\phi_{c,k}(x)q_{c,k}(t)-\frac{1}{2}\sum_{k=\pm1}^{\pm N_{vv}}T\phi_{vv,k}q_{vv,k}(t)-\sum_{k=1}^{N_{vr}}T\phi_{vr,j}q_{vr,k}(t)\right\}\\&+C_{cv}\left\{\frac{1}{2}\sum_{k=\pm1}^{\pm\infty}\Pi_x\left[x_{cv}(t)\right]\phi_{c,k}(x)\dot{q}_{c,k}(t)-\frac{1}{2}\sum_{k=\pm1}^{\pm N_{vv}}T\phi_{vv,k}\dot{q}_{vv,k}(t)-\sum_{k=1}^{N_{vr}}T\phi_{vr,j}\dot{q}_{vr,k}(t)\right\}\\&+C_{cv}\frac{1}{2}\sum_{k=\pm1}^{\pm\infty}\frac{d\Pi_x\left[x_{cv}(t)\right]\phi_{c,k}(x)}{dt}q_{c,k}(t)\end{aligned} \tag{24}$$

Using Eq. (24), the modal interaction forces can be obtained [Eq. (21)] and substituted into Eq. (23) yielding a set of linear ordinary differential equations with time dependent coefficients for the modal coordinates. Additionally, the modal input terms due to initial conditions [Eq. (19)] can be recognized to be equivalent to the initial conditions for the unknown modal coordinates:

$$q_{c,k}(0) = \frac{1}{\lambda_{c,k}} \dot{q}_{c0,k} + q_{c0,k}, \; k = \pm 1, \pm 2, \ldots \tag{25a}$$

$$q_{vv,k}(0) = \frac{1}{\lambda_{vv,k}} \dot{q}_{vv0,k} + q_{vv0,k}, \; k = \pm 1, \pm 2, \ldots, \pm N_{vv} \tag{25b}$$

$$q_{vr,k}(0) = q_{vr0,k}, \; \dot{q}_{vr,k}(0) = \dot{q}_{vr0,k}, \; k = 1, 2, \ldots, N_{vr} \tag{25c, d}$$

Thus, the final set of equations for the modal coordinates is as follows:

$$\dot{q}_{c,k}(t) - \lambda_{c,k} q_{c,k}(t) + \frac{\left\{\Pi_x\left[x_{cv}(t)\right]\bar{\psi}_{c,k}(x)\right\}^T}{\lambda_{c,k}} y(t) = \frac{Q_{c,k}(t)}{\lambda_{c,k}}, \; k = \pm 1, \pm 2, \ldots \tag{26a}$$

$$\dot{q}_{vv,k}(t) - \lambda_{vv,k} q_{vv,k}(t) - \frac{\bar{\psi}_{vv,k}^T T^T}{\lambda_{vv,k}} y(t) = \frac{Q_{vv,k}(t)}{\lambda_{vv,k}}, \; k = \pm 1, \pm 2, \ldots, \pm N_{vv} \tag{26b}$$

$$\ddot{q}_{vr,k}(t) - \psi_{vr,k}^T T^T y(t) = Q_{vr,k}(t), \; k = 1, 2, \ldots, N_{vr} \tag{26c}$$

and the initial conditions are given by Eq. (25).

Expanding Eq. (12) and substituting into it Eq. (22), the solution for the interaction problem, i.e., the response of the continuum and vehicle, can be found as:

$$u_c(x,t) = \frac{1}{2} \sum_{k=\pm 1}^{\pm\infty} \phi_{c,k}(x) q_{c,k}(t) \tag{27a}$$

$$u_v(t) = \frac{1}{2} \sum_{k=\pm 1}^{\pm N_{vv}} \phi_{vv,k} q_{vv,k}(t) + \sum_{k=1}^{N_{vr}} \phi_{vr,k} q_{vr,k}(t) \tag{27b}$$

Equations (26) and (27) represent an exact solution of the problem of the interaction of a non-self-adjoint, MDOF oscillator moving over a non-self-adjoint, 1D continuum, and interacting with it through linear elastic and viscous forces. For practical applications, the number of equations in Eq. (26a) must always be truncated, and the problem is reduced to solving a finite-dimensional set of differential equations.

2.4. Real Form for the Solution

Equations (26) governing the modal coordinates have complex valued coefficients. In order to avoid complex arithmetic, a real form of the solution is desirable. The notation used in this section is such that superscripts "*R*" and "*I*" denote the real and imaginary part of the superscripted complex quantity, respectively. The real form of Eq. (26) is

$$\dot{q}^R_{c,k}(t) - \lambda^R_{c,k} q^R_{c,k}(t) + \lambda^I_{c,k} q^I_{c,k}(t) + \frac{\lambda^R_{c,k}\left\{\Pi_x\left[x_{cv}(t)\right]\psi^R_{c,k}(x)\right\}^T - \lambda^I_{c,k}\left\{\Pi_x\left[x_{cv}(t)\right]\psi^I_{c,k}(x)\right\}^T}{\left|\lambda_{c,k}\right|^2} y(t) =$$

$$= \frac{\lambda^R_{c,k} Q^R_{c,k}(t) + \lambda^I_{c,k} Q^I_{c,k}(t)}{\left|\lambda_{c,k}\right|^2}$$

$$k = 1,\ 2,\ \ldots \tag{28a}$$

$$\dot{q}^I_{c,k}(t) - \lambda^I_{c,k} q^R_{c,k}(t) - \lambda^R_{c,k} q^I_{c,k}(t) - \frac{\lambda^I_{c,k}\left\{\Pi_x\left[x_{cv}(t)\right]\psi^R_{c,k}(x)\right\}^T + \lambda^R_{c,k}\left\{\Pi_x\left[x_{cv}(t)\right]\psi^I_{c,k}(x)\right\}^T}{\left|\lambda_{c,k}\right|^2} y(t) =$$

$$= \frac{\lambda^R_{c,k} Q^I_{c,k}(t) - \lambda^I_{c,k} Q^R_{c,k}(t)}{\left|\lambda_{c,k}\right|^2}$$

$$k = 1,\ 2,\ \ldots \tag{28b}$$

$$\dot{q}^R_{vv,k}(t) - \lambda^R_{vv,k} q^R_{vv,k}(t) + \lambda^I_{vv,k} q^I_{vv,k}(t) - \frac{\lambda^R_{vv,k}\psi^R_{vv,k}{}^T T^T - \lambda^I_{vv,k}\psi^I_{vv,k}{}^T T^T}{\left|\lambda_{vv,k}\right|^2} y(t) = \frac{\lambda^R_{vv,k} Q^R_{vv,k}(t) + \lambda^I_{vv,k} Q^I_{vv,k}(t)}{\left|\lambda_{vv,k}\right|^2}$$

$$k = 1,\ 2,\ \ldots,\ N_{vv} \tag{28c}$$

$$\dot{q}^I_{vv,k}(t)-\lambda^I_{vv,k}q^R_{vv,k}(t)-\lambda^R_{vv,k}q^I_{vv,k}(t)+\frac{\lambda^I_{vv,k}\psi^R_{vv,k}{}^T T^T+\lambda^R_{vv,k}\psi^I_{vv,k}{}^T T^T}{\left|\lambda_{vv,k}\right|^2}y(t)=\frac{\lambda^R_{vv,k}Q^I_{vv,k}(t)-\lambda^I_{vv,k}Q^R_{vv,k}(t)}{\left|\lambda_{vv,k}\right|^2}$$

$$k=1,\ 2,\ \ldots,\ N_{vv} \tag{28d}$$

$$\ddot{q}_{vr,k}(t)-\psi^T_{vr,k}T^T y(t)=Q_{vr,k}(t),\ k=1,2,\ldots,N_{vr} \tag{28e}$$

The interaction forces $y(t)$ are given in terms of the real and imaginary parts of the modal coordinates as

$$\begin{aligned}
y(t)=K_{cv}&\left\{\sum_{k=1}^{\infty}\left\{\Pi_x\left[x_{cv}(t)\right]\phi^R_{c,k}(x)q^R_{c,k}(t)-\Pi_x\left[x_{cv}(t)\right]\phi^I_{c,k}(x)q^I_{c,k}(t)\right\}\right.\\
&\left.-\sum_{k=1}^{N_{vv}}\left\{T\phi^R_{vv,k}q^R_{vv,k}(t)-T\phi^I_{vv,k}q^I_{vv,k}(t)\right\}-\sum_{k=1}^{N_{vr}}T\phi_{vr,j}q_{vr,k}(t)\right\}\\
&+C_{cv}\left\{\sum_{k=1}^{\infty}\left\{\Pi_x\left[x_{cv}(t)\right]\phi^R_{c,k}(x)\dot{q}^R_{c,k}(t)-\Pi_x\left[x_{cv}(t)\right]\phi^I_{c,k}(x)\dot{q}^I_{c,k}(t)\right\}\right.\\
&\left.-\sum_{k=1}^{N_{vv}}\left\{T\phi^R_{vv,k}\dot{q}^R_{vv,k}(t)-T\phi^I_{vv,k}\dot{q}^I_{vv,k}(t)\right\}-\sum_{k=1}^{N_{vr}}T\phi_{vr,j}\dot{q}_{vr,k}(t)\right\}\\
&+C_{cv}\sum_{k=1}^{\infty}\left\{\frac{d\Pi_x\left[x_{cv}(t)\right]\phi^R_{c,k}(x)}{dt}q^R_{c,k}(t)-\frac{d\Pi_x\left[x_{cv}(t)\right]\phi^I_{c,k}(x)}{dt}q^I_{c,k}(t)\right\}
\end{aligned} \tag{29}$$

while the initial conditions are as follows:

$$q^R_{c,k}(0)=\frac{\lambda^R_{c,k}\dot{q}^R_{c0,k}-\lambda^I_{c,k}\dot{q}^I_{c0,k}}{\left|\lambda_{c,k}\right|^2}+q^R_{c0,k},\ q^I_{c,k}(0)=\frac{\lambda^I_{c,k}\dot{q}^R_{c0,k}+\lambda^R_{c,k}\dot{q}^I_{c0,k}}{\left|\lambda_{c,k}\right|^2}+q^I_{c0,k},\ k=1,\ 2,\ \ldots \tag{30a, b}$$

$$q^R_{vv,k}(0)=\frac{\lambda^R_{vv,k}\dot{q}^R_{vv0,k}-\lambda^I_{vv,k}\dot{q}^I_{vv0,k}}{\left|\lambda_{vv,k}\right|^2}+q^R_{vv0,k},\ q^I_{vv,k}(0)=\frac{\lambda^I_{vv,k}\dot{q}^R_{vv0,k}+\lambda^R_{vv,k}\dot{q}^I_{vv0,k}}{\left|\lambda_{vv,k}\right|^2}+q^I_{vv0,k}$$

$$k=1,\ 2,\ \ldots,\ N_{vv} \tag{30c, d}$$

and external modal forces as follows:

$$Q^R_{c,k}(t)=\int_{-\infty}^{\infty}\psi^R_{c,k}(x)\,f_c(x,t)\,\mathrm{d}x,\ Q^I_{c,k}(t)=-\int_{-\infty}^{\infty}\psi^I_{c,k}(x)\,f_c(x,t)\,\mathrm{d}x,\ k=1,\ 2,\ \ldots \tag{31a, b}$$

$$Q_{vv,k}^{R}(t)=\psi_{vv,k}^{R\ T}f_v(t),\ Q_{vv,k}^{I}(t)=-\psi_{vv,k}^{I\ T}f_v(t),\ k=1,\ 2,\ \ldots,\ N_{vv} \tag{31c, d}$$

The solution for the interaction problem can now be written as follows:

$$u_c(x,t)=\sum_{k=1}^{\infty}\left[\phi_{c,k}^{R}(x)q_{c,k}^{R}(t)-\phi_{c,k}^{I}(x)q_{c,k}^{I}(t)\right] \tag{32a}$$

$$u_v(t)=\sum_{k=1}^{N_{vv}}\left[\phi_{vv,k}^{R}q_{vv,k}^{R}(t)-\phi_{vv,k}^{I}q_{vv,k}^{I}(t)\right]+\sum_{k=1}^{N_{vr}}\phi_{vr,k}q_{vr,k}(t) \tag{32b}$$

2.5. Special Case: Proportionally Damped Systems

A special case of the interaction problem is concerned with proportionally damped systems. For such systems, the following conditions hold ([14], [16]): i) $\hat{C}_c=\hat{C}_c^{*}$ and $\hat{K}_c=\hat{K}_c^{*}$, ii) $\hat{C}_c\hat{M}_c^{-1}\hat{K}_c z(x)=\hat{K}_c\hat{M}_c^{-1}\hat{C}_c z(x)$ for any sufficiently differentiable function $z(x)$, iii) the boundary conditions of the higher order operator of $\hat{C}_c$ and $\hat{K}_c$ are derivable from a compatible set of boundary conditions of the lower order operator, iv) $C_v=C_v^{T}$ and $K_v=K_v^{T}$, and v) $C_vM_v^{-1}K_v=K_vM_v^{-1}C_v$. As can easily be seen from Eqs. (8) and (10), the solutions for the direct and adjoint eigenvalue problems for proportionally damped systems coincide. The eigenfunctions of the continuum and eigenvectors of the oscillator are real and will be denoted by $\varphi_{c,k}(x)$ ($k=1,\ 2,\ \ldots$) and $\varphi_{v,k}$ ($k=1,\ 2,\ \ldots,\ N_v$), respectively. Note that differentiating the notation for the oscillator's vibratory and rigid modes is now not necessary, and the total number of oscillator's modes is $N_v=N_{vv}+N_{vr}$. The eigenfunctions and eigenvectors of the proportionally damped systems are usually normalized as follows:

$$\int_0^L\varphi_{c,k}(x)\hat{M}_c\varphi_{c,k}(x)\,\mathrm{d}x=1,\ k=1,\ 2,\ \ldots \tag{33a}$$

$$\varphi_{v,k}^{T}M_v\varphi_{v,k}=1,\ k=1,\ 2,\ \ldots,\ N_v \tag{33b}$$

To derive the equations for the modal coordinates one can substitute $\varphi_{c,k}(x)$ and $\varphi_{v,k}$ for $\phi_{c,k}(x)$, $\phi_{vv,k}$ and $\phi_{vr,k}$. However, as shown by Pesterev and Bergman ([11]), except for conservative systems, if the normalization conditions of Eqs. (9) and (11a) are to hold, $\psi_{c,k}(x)$ and $\psi_{vv,k}$ must be substituted for by $c_{c,k}\varphi_{c,k}(x)$ and $c_{vv,k}\varphi_{vv,k}$, where complex constants $c_{c,k}$ and $c_{vv,k}$ are as follows:

$$c_{c,k} = i\frac{\bar{\lambda}_{c,k}}{\lambda^{I}_{c,k}},\ k=1,\ 2,\ \ldots \tag{34a}$$

$$c_{vv,k} = i\frac{\bar{\lambda}_{vv,k}}{\lambda^{I}_{vv,k}},\ k=1,\ 2,\ \ldots,\ N_{vv} \tag{34b}$$

where *i* denotes the imaginary unit. Differentiating Eq. (28a) and substituting into it Eq. (28b), and performing the same procedure for Eqs. (28c) and (28d) yields second order differential equations for the real parts of modal coordinates (note that superscript "*R*" was dropped for brevity):

$$\ddot{q}_{c,k}(t) + 2\zeta_{c,k}\omega_{0c,k}\dot{q}_{c,k}(t) + \omega^2_{0c,k}q_{c,k}(t) + \left\{\Pi_x\left[x_{cv}(t)\right]\varphi_{c,k}(x)\right\}^T y(t) = Q_{c,k}(t),\ k=1,\ 2,\ \ldots \tag{35a}$$

$$\ddot{q}_{v,k}(t) + 2\zeta_{v,k}\omega_{0v,k}\dot{q}_{v,k}(t) + \omega^2_{0v,k}q_{v,k}(t) - \varphi^T_{v,k}T^T y(t) = Q_{v,k}(t),\ k=1,\ 2,\ \ldots,\ N_v \tag{35b}$$

with interaction forces:

$$\begin{aligned} y(t) = {} & K_{cv}\left\{\sum_{k=1}^{\infty}\Pi_x\left[x_{cv}(t)\right]\varphi_{c,k}(x)q_{c,k}(t) - \sum_{k=1}^{N_v}T\varphi_{v,k}q_{v,k}(t)\right\} \\ & + C_{cv}\left\{\sum_{k=1}^{\infty}\Pi_x\left[x_{cv}(t)\right]\varphi_{c,k}(x)\dot{q}_{c,k}(t) - \sum_{k=1}^{N_v}T\varphi_{v,k}\dot{q}_{v,k}(t)\right\} \\ & + C_{cv}\sum_{k=1}^{\infty}\left\{\frac{d\Pi_x\left[x_{cv}(t)\right]\varphi_{c,k}(x)}{dt}q_{c,k}(t)\right\} \end{aligned} \tag{36}$$

external modal forces:

$$Q_{c,k}(t) = \int_{-\infty}^{\infty} \varphi_{c,k}(x)\, f_c(x,t)\,\mathrm{d}x\,,\ k = 1,\ 2,\ \ldots \tag{37a}$$

$$Q_{v,k}(t) = \varphi_{v,k}^T f_v(t)\,,\ k = 1,\ 2,\ \ldots,\ N_v \tag{37b}$$

and initial conditions:

$$q_{c,k}(0) = \int_{-\infty}^{\infty} \varphi_{c,k}(x)\hat{M}_c u_c(x,0)\,\mathrm{d}x\,,\ \dot{q}_{c,i}(0) = \int_{-\infty}^{\infty} \varphi_{c,k}(x)\hat{M}_c \dot{u}_c(x,0)\,\mathrm{d}x\,,\ k = 1,\ 2,\ \ldots \tag{38a, b}$$

$$q_{v,k}(0) = \varphi_{v,k}^T(x) M_v u_c(0)\,,\ \dot{q}_{v,k}(0) = \varphi_{v,k}^T(x) M_v \dot{u}_c(0)\,,\ k = 1,\ 2,\ \ldots,\ N_v \tag{38c, d}$$

Symbols $\omega_{0,k}$ and ζ_k represent undamped natural frequencies and damping ratios, respectively, and can be defined for the continuum and the vehicle as follows:

$$\omega_{0c,k} = \left|\lambda_{c,k}\right|,\ \zeta_{c,k} = -\frac{\lambda_{c,k}^R}{\left|\lambda_{c,k}\right|},\ k = 1,\ 2,\ \ldots \tag{39a, b}$$

$$\omega_{0v,k} = \left|\lambda_{v,k}\right|,\ \zeta_{v,k} = \begin{cases} -\dfrac{\lambda_{v,k}^R}{\left|\lambda_{v,k}\right|} & \text{for } \left|\lambda_{v,k}\right| \neq 0 \\ 0 & \text{for } \left|\lambda_{v,k}\right| = 0 \end{cases},\ k = 1,\ 2,\ \ldots,\ N_v \tag{39c, d}$$

The solution for the interaction problem in the case of proportionally damped systems can be found as

$$u_c(x,t) = \sum_{k=1}^{\infty} \varphi_{c,k}(x) q_{c,k}(t) \tag{40a}$$

$$u_v(t) = \sum_{i=1}^{N_v} \varphi_{v,k} q_{v,k}(t) \tag{40b}$$

The results for the proportionally damped systems described in this section have been obtained previously by Omenzetter and Fujino ([12]) under more restricting assumptions. Here they are presented as a special case of the general interaction problem considered.

3. NUMERICAL EXAMPLES

In order to explain the application of the introduced mathematical concepts and study selected numerical aspects of the proposed method, such as convergence, two detailed numerical examples are provided.

3.1. Example 1

The purpose of this example is twofold: i) to offer a "guided tour" explaining the application of the theory to a particular system with the various operators explicitly shown for the system at hand, and ii) to obtain insights about the rate of numerical convergence for simple systems such as Euler-Bernoulli beams with uniformly distributed parameters.

The continuum is a proportionally damped, simply supported Euler-Bernoulli beam studied previously by Green and Cebon ([4]), with length $L = 40\,\mathrm{m}$, constant bending stiffness $EI = 1.275\times10^{11}\ \mathrm{Nm}^2$ and mass per unit length $m = 1.2\times10^{4}\ \mathrm{kg/m}$. Models of this type are often use for analysis of vibrations in simple bridge structures.

The operator governing the motion of the isolated beam is

$$\hat{A}_c u_c(x,t) = m\frac{\partial^2 u_c(x,t)}{\partial t^2} + \left(\alpha_1 m + \alpha_2 EI\,\frac{\partial^4}{\partial x^4}\right)\frac{\partial u_c(x,t)}{\partial t} + EI\,\frac{\partial^4 u_c(x,t)}{\partial x^4} \tag{41}$$

where the damping operator, $\hat{C}_c = \alpha_1 m + \alpha_2 EI\,\partial^4/\partial x^4$, was chosen to represent the Rayleigh proportional damping ([17]), and the numerical coefficients, $\alpha_1 = 0.6434\ s^{-1}$ and $\alpha_2 = 0.0004\ s$, were selected in agreement with the example of Green and Cebon ([4]). The eigenfunctions, undamped natural frequencies and damping ratios are as follows:

$$\varphi_{c,k}(x) = \sqrt{\frac{2}{mL}}\sin\frac{k\pi x}{L},\ \omega_{0c,k} = \left(\frac{k\pi}{L}\right)^2\sqrt{\frac{EI}{m}},\ \zeta_{c,k} = \frac{\alpha_1}{2\omega_{0c,k}} + \frac{\alpha_2\omega_{0c,k}}{2},\ k = 1,\ 2,\ \ldots \text{(42a-c)}$$

The external forces acting on the beam are ignored and the beam is assumed to be at rest before the oscillator arrival.

The vehicle and interaction models are depicted in Fig. 2. The masses are $m_1 = 3.6\times10^4$ kg and $m_2 = m_3 = 2.0\times10^3$ kg, the second-order mass moment of inertia is $I_1 = 1.44\times10^5$ kgm^2, the spring stiffness values are $k_1 = k_2 = 9.0\times10^6$ N/m, and damping coefficients are $c_1 = 7.92\times10^4$ kg/s and $c_2 = 7.2\times10^4$ kg/s. The values of interaction spring stiffness are $k_3 = k_4 = 3.6\times10^7$ N/m and damping coefficients are $c_3 = c_4 = 7.2\times10^4$ kg/s. The distance between axles is $l = 1.0$ m. The vector of displacements of this 4DOF vehicle model, $u_v^T(t) = \left[u_{v,1} \quad u_{v,2} \quad u_{v,3} \quad u_{v,4}\right]$, consist of sprung mass (vehicle body) displacement, sprung mass pitch rotation and two tire displacements. The zero displacement vector corresponds to the state when no forces exist in the vehicle and interaction model springs. The mass, damping and stiffness matrices appearing in operator $\hat{A}_v$ [Eq. (3b)] are as follows:

$$M_v = \begin{bmatrix} m_1 & 0 & 0 & 0 \\ & I_1 & 0 & 0 \\ & & m_2 & 0 \\ sym. & & & m_3 \end{bmatrix},\ C_v = \begin{bmatrix} c_1+c_2 & -(c_1-c_2)l/2 & -c_1 & -c_2 \\ & (c_1+c_2)l^2/2 & c_1 l/2 & -c_2 l/2 \\ & & c_1 & 0 \\ sym. & & & c_2 \end{bmatrix} \qquad \text{(43a, b)}$$

$$K_v = \begin{bmatrix} k_1+k_2 & -(k_1-k_2)l/2 & -k_1 & -k_2 \\ & (k_1+k_2)l^2/4 & k_1 l/2 & -k_2 l/2 \\ & & k_1 & 0 \\ sym. & & & k_2 \end{bmatrix} \qquad \text{(43c)}$$

The above mass, damping and stiffness matrices describe, in a general case as well as for the particular selection of mechanical parameter values considered here, a non-proportionally damped system. The eigenvalues of the vehicle model are as follows: for the rigid body modes $\lambda_{vr,1} = \lambda_{vr,2} = 0$ rad/s, and for the oscillatory modes $\lambda_{vv,1} = (-19.02 + 64.86i)$ rad/s and

$\lambda_{vv,2} = \left(-21.02 + 67.21i\right)\,\mathrm{rad/s}$. The eigenvectors of the direct eigenvalue problem corresponding to the rigid body modes are $\phi_{vr,1}^T = \left[-0.500 \quad 1.000 \quad -1.000 \quad 0.000\right]$ and $\phi_{vr,2}^T = \left[0.667 \quad 0.667 \quad 0.333 \quad 1.000\right]$. These are, however, not uniquely determined and any linear combination of $\phi_{vr,1}$ and $\phi_{vr,2}$ also represents a rigid body mode. The eigenvectors of the direct eigenvalue problem corresponding to the oscillatory modes are $\phi_{vv,1}^T = \left[-0.093 + 0.025i \quad 0.002 + 0.003i \quad 1.000 \quad 0.674 - 0.456i\right]$ and $\phi_{vv,2}^T = \left[-0.015 - 0.023i \quad -0.012 + 0.003i \quad -0.730 + 0.416i \quad 1.000\right]$. Since the vehicle model is non-gyroscopic and non-circulatory, i.e., $C_v = C_v^T$ and $K_v = K_v^T$, the eigenvectors of the adjoint eigenvalue problem can easily be found as $\psi_{vr,1} = \phi_{vr,1}$, $\psi_{vr,2} = \phi_{vr,2}$, $\psi_{vv,1} = \bar{\phi}_{vv,1}$ and $\psi_{vv,2} = \bar{\phi}_{vv,2}$, however they need to be later normalized so that the conditions of Eqs. (11a) and (11b) are satisfied. The external forces acting on the vehicle are the gravity forces, i.e., $f_v^T = \left[m_1 g \quad 0 \quad m_2 g \quad m_3 g\right]$, where g is the gravity acceleration. The initial displacements of the vehicle due to the presence of gravity forces can be computed as $u_v(0) = \left(K_v + T^T K_{cv} T\right)^{-1} f_v$, where matrices K_{cv} and T are shown in the following paragraph; the initial velocities are assumed to be zero.

The stiffness and damping matrices that describe the interaction forces are as follows: $K_{cv} = \mathrm{diag}\left(k_3,\ k_4\right)$ and $C_{cv} = \mathrm{diag}\left(c_3,\ c_4\right)$, whereas matrix T is as follows:

$$T = \begin{bmatrix} 0 & 0 & 1 & 0 \\ 0 & 0 & 0 & 1 \end{bmatrix} \tag{44}$$

Assuming that the velocity of the vehicle, v, is constant and that the zero time corresponds to the instant when the front axle enters the beam, the vector of contact point location is given as

$x_{cv}(t) = [vt - l \quad vt]^T$, and the action of the sensor operator $\Pi_x[x_{cv}(t)]$ on an eigenfunction $\varphi_{c,k}(x)$ when $l/v \le t \le L/v$ results in

$$\left\{\Pi_x[x_{cv}(t)]\varphi_{c,k}(t)\right\}^T = \sqrt{\frac{2}{mL}}\left[\sin\frac{k\pi(vt-l)}{L} \quad \sin\frac{k\pi vt}{L}\right]^T,\ k = 1,\ 2,\ \ldots \qquad (45)$$

The integration of equations of motion was carried out using a Runge-Kutta method ([18]).

For practical applications, the number of modes of the continuum taken into account must be finite and will be denoted by N_c. The numerical example examines the convergence of the solution with increasing N_c. Figures 3 and 4 show the results of the simulations for an oscillator travelling with a constant speed of $v = 25$ m/s. In Fig. 3, mid-span deflections, $u_c(0.5L, t)$, obtained with one, two or three beam modes considered are shown, whereas Fig. 4 shows the vehicle body displacements, $u_{v,1}(t)$. It can be seen that a very good approximation is obtained for a small number of beam modes taken into account – the addition of the third mode changes the maximum mid-span beam deflection by only 1.3% compared to the approximation using two modes, and all maximum vehicle displacements by less than 1.0%.

3.2. Example 2

The second example is concerned with a more complex continuum and a situation where both the oscillator and the continuum are non-proportionally damped systems with complex modes. The discussion focuses on the estimation of continuum complex eigenfunctions and the rate of convergence of the solution to the dynamic interaction problem. The vehicle model is the same as considered in Example 1 and all other parameters and approaches are to be assumed unaltered unless indicated otherwise.

The continuum is an Euler-Bernoulli beam on a Winkler-type viscoelastic foundation shown in Fig. 5. Similar models are often employed to study response of railway tracks to moving trains ([19, 20]). Numerical values were adopted from their respective typical ranges discussed in [20]. The beam is assumed to be simply supported, its length is $L = 20\,\mathrm{m}$, bending stiffness is $EI = 1.22\times10^{7}\ \mathrm{Nm}^2$ and mass per unit length is $m = 120.7\,\mathrm{kg/m}$. The beam is assumed undamped, as for the typical values of rail and foundation damping the latter is dominant. The foundation stiffness, $k(x)$, varies along the beam length as follows:

$$k(x) = \begin{cases} k_1 = 0.5\times10^{7}\ N/m^2 & for\ |x - L/2| > a \\ k_2 = 0.7\times10^{7}\ N/m^2 & for\ |x - L/2| \le a \end{cases} \tag{46}$$

i.e., the segment of length $2a$ located centrally in the middle of the beam has a larger stiffness compared to the end segments, each $L/2 - a$ long. Foundation damping is assumed proportional to its stiffness $c(x) = \gamma k(x)$, where $\gamma = 0.001\,m^{-1}s^{-1}$. In the numerical analyses, three cases of the stiffer middle segment length were considered, namely Case 1: $a = L/12$, Case 2: $a = L/6$, and Case 3: $a = L/4$.

The operator governing the motion of the beam on viscoelastic foundation is ([20]):

$$\hat{A}_c u_c(x,t) = m\frac{\partial^2 u_c(x,t)}{\partial t^2} + c(x)\frac{\partial u_c(x,t)}{\partial t} + \left(EI\frac{\partial^4}{\partial x^4} + k(x)\right)u_c(x,t) \tag{47}$$

It can easily be verified that the proportional damping conditions of [14], also quoted in Section 2.5 of this paper, do not hold, and consequently the continuum mode shapes are complex. The Galerkin method was employed to approximate the complex modes of the continuum. The theory and procedural steps of the method are presented in, e.g., [17] and herein only a brief explanation and relevant details are included. The continuum

eigenfunctions were resolved using the eigenfunctions of an undamped, uniform, simply supported Euler-Bernoulli beam as comparison functions:

$$\phi_{c,k}^{(N_G)}(x) = \sum_{s=1}^{N_G} p_{k,s}^{(N_G)} \sin\frac{s\pi x}{L},\ k = 1, 2, \ldots, N_G \tag{48}$$

where N_G is the number of comparison functions used in the Galerkin approximation, and $p_{k,s}^{(N_G)}$ are approximation coefficients. N_G used as a superscript in parentheses emphasizes that approximations themselves and coefficients involved in the related formulas depend on the number of terms used in Eq. (48). Substituting Eq. (48) into Eq. (8a) and minimizing the residual error of the approximate eigenvalue problem solution discretises the eigenvalue problem as follows:

$$\left(\left(\lambda_{c,k}^{(N_G)}\right)^2 M_c^{(N_G)} + \lambda_{c,k}^{(N_G)} C_c^{(N_G)} + K_c^{(N_G)}\right) p_{k,s}^{(N_G)} = 0,\quad k, s = 1, 2, \ldots, N_G \tag{49}$$

The entries of matrices $M_c^{(N_G)}$, $C_c^{(N_G)}$ and $K_c^{(N_G)}$ are as follows:

$$M_{c,ks}^{(N_G)} = \frac{mL}{2}\delta_{ks},\quad k, s = 1, 2, \ldots, N_G \tag{50a}$$

$$C_{c,ks}^{(N_G)} = \int_0^L c(x) \sin\frac{k\pi x}{L} \sin\frac{s\pi x}{L} dx,\quad k, s = 1, 2, \ldots, N_G \tag{50b}$$

$$K_{c,ks}^{(N_G)} = \int_0^L \sin\frac{k\pi x}{L}\left(EI\frac{\partial^4}{\partial x^4} + k(x)\right)\sin\frac{s\pi x}{L} dx,\quad k, s = 1, 2, \ldots, N_G \tag{50c}$$

where the Kronecker delta δ_{ks} equals 1 only when $k = s$, and 0 otherwise.

Table 1 lists the undamped natural frequencies (in unit of Hz) and damping ratios for the first 10 modes for foundation stiffness Case 1, 2 and 3, approximated by the Galerkin method with $N_G = 12$. (It will be demonstrated later that these choices of the number of modes

and Galerkin terms, respectively, assured satisfactory accuracy for all considered numerical cases.) It can be seen that those frequencies are closely spaced, e.g., there are as many as 10 modes between 30 Hz and 130 Hz. The large number of closely spaced frequencies can be explained as follows: Assuming for convenience no damping and uniform foundation stiffness $k(x)=k$, the natural frequencies are, after [20], given by $\omega_{0c,n}=\sqrt{\left(n^4\pi^4 EI/L^4+k\right)/m}$, $n=1,\ 2,\ \ldots$. For the chosen order of stiffness values, the contribution of foundation, which does not depend on mode number, dominates over that of the beam for lower modes. Also, it can be seen from Table 1 that damping ratios are of the order of 8-12% for the lowest five modes, and for higher modes gradually decrease to about 3% for the tenth mode. Figures 6 and 7 show, respectively, the real and imaginary parts of the first three right mode shapes. Note that for easier comparison the modes have been scaled such that the largest value of real part is one. It is interesting to notice that increasing the length of the stiffer foundation part between Case 1 and 2 leads to a switch of mode order and the lowest antisymmetric mode becomes the lowest mode overall. The first symmetric mode shape appears to be particularly strongly affected by the non-uniform stiffness distribution. For a uniform foundation stiffness distribution, this mode would have a half-sine shape but for all considered cases it is now M-shaped. Comparing the magnitudes of the real and imaginary parts it can be seen that the latter never exceed 10% of the former. A general trend of some small increase in the magnitudes of the imaginary parts can also be observed as one moves from Case 1 through to Case 3.

Tables 2 and 3 demonstrate the rate of convergence of eigenvalues and eigenvectors, respectively, with increasing number of terms, N_G, in the Galerkin solution for Case 1 of foundation stiffness. The reported errors were calculated as relative percentage differences between approximations using N_G+2 and N_G terms. (The comparison between the N_G+1

and N_G term approximations would not be meaningful as the addition of another symmetric comparison function does not affect antisymmetric modes and vice versa.) The formulas for eigenvalue and eigenfunction errors are respectively as follows:

$$e_{\lambda,k}^{(N_G+2)} = \left| \frac{\lambda_{c,k}^{(N_G+2)} - \lambda_{c,k}^{(N_G)}}{\lambda_{c,k}^{(N_G+2)}} \right| \times 100\% \tag{51}$$

$$e_{\phi,k}^{(N_G+2)} = \sqrt{\frac{\int_0^L \left(\bar{\phi}_{c,k}^{(N_G+2)}(x) - \bar{\phi}_{c,k}^{(N_G)}(x) \right) \left(\phi_{c,k}^{(N_G+2)}(x) - \phi_{c,k}^{(N_G)}(x) \right) dx}{\int_0^L \bar{\phi}_{c,k}^{(N_G+2)}(x) \phi_{c,k}^{(N_G+2)}(x) dx}} \times 100\% \tag{52}$$

It can be seen that with $N_G = 12$ the errors are small, not exceeding 0.005% and 0.56% for the lowest 10 eigenvalues and eigenvectors, respectively. Similar conclusions were drawn for the two remaining foundation stiffness cases and also for the adjoint eigenvalue problem. This confirms that the choice of $N_G = 12$ provides satisfactory accuracy for the first 10 modes.

Table 4 illustrates the convergence of time history numerical integration with increasing numbers of modes, N_C, retained in the system of equations of motion [Eq.(28)] for Case 1 of foundation stiffness. The maximum mid-span beam deflections are listed in the second row, and the third row shows relative percentage differences, or errors, between approximations using $N_C + 1$ and N_C modes. This point-wise convergence is non-monotonic and relatively slow as compared to Example 1 – 10 modes are required to reduce the error between subsequent approximations to below 1% (where it later stays, although this is omitted from the table). Figure 8 shows the full time histories of mid-span deflection, $u_c(0.5L, t)$, for $N_C = 1, 3, 5, 7, 9$ and 10 modes taken into account for Case 1 of foundation stiffness. It can be seen that, unless at least five modes are used, the shape of time history plot in the middle

portion of the figure (approximately from $0.27s$ to $0.57s$) cannot even be qualitatively captured, as solutions with less modes indicate two peaks. With five or more mode shapes, the correct, single peak shape is obtained, and convergence to the maximum value becomes clearly visible. It is also noted that the parts of the time histories just after the vehicle enters the beam, before approximately $0.27s$, and just before it leaves it, after approximately $0.57s$, show large variations with the number of modes. Using five modes, predicts that those displacements will be both negative and positive, whereas using more modes show them to be only negative. However, those displacements are not the extreme values and so this slower convergence is more tolerable from the point of view of practical applications.

Figures 9 and 10 examine the contribution of real, $q_{c,k}^{R}(t)$, and imaginary part, $q_{c,k}^{I}(t)$, respectively, of modal coordinates (see Eq.(32a)) of the first three modes to the response in the middle of the beam, $u_c(0.5L,t)$, for the three cases of stiffer foundation length. It can be seen that the maximum magnitudes of the imaginary parts are about 10% of the maximum magnitudes of the real parts, a proportion that is similar to that of the real and imaginary parts of mode shapes themselves, shown in Fig. 6 and 7. Some small decrease in the magnitudes of the real parts and increase in the magnitudes of the imaginary parts can also be observed as one moves from Case 1 through to Case 3.

4. CONCLUSIONS

A method for computing the response of a 1D elastic continuum induced by a MDOF oscillator travelling over it has been proposed. The continuum and the oscillator are both non-self-adjoint systems and the interaction between them is through linear elastic and viscous forces. An exact solution has been obtained in the form of a series using eigenfunctions and

eigenvectors of the isolated continuum and oscillator, respectively. It is noted that when exact eigenvalues and eigenfunctions of the continuum are not available their approximations can be used. The time dependent terms of the series are solutions of a system of linear differential equations with time dependent coefficients. The coefficients of these equations depend on eigenvalues as well as eigenfunctions and eigenvectors of the isolated continuum and the oscillator, and stiffness and damping of the interaction elements. The method has been applied to two numerical examples which demonstrate its use and study convergence.

REFERENCES

[1] Chatterjee, P. K., Datta, T. K., and Surana, C. S., 1994, "Vibration of Suspension Bridges under Vehicular Movement," *ASCE Journal of Structural Engineering*, 120, No. 3, pp. 681-703.

[2] Fryba, L., 1972, *Vibration of Solids and Structures under Moving Loads*, Noordhoff International Publishing, Groningen, The Netherlands.

[3] Fryba, L., 1996, *Dynamics of Railway Bridges*, Thomas Telford, London, Great Britain.

[4] Green, M. F., and Cebon, D., 1994, "Dynamic Response of Highway Bridges to Heavy Vehicle Loads: Theory and Experimental Validation," *Journal of Sound and Vibration*, 170, No. 1, pp. 51-78.

[5] Sadiku, S., and Leipholz, H. H. E., 1987, "On the Dynamics of Elastic Systems with Moving Concentrated Masses," *Ingenieur Archiv*, 57, pp. 223-242.

[6] Stanišić, M. M, 1985, "On a New Theory of the Dynamic Behavior of the Structures Carrying Moving Masses," *Ingenieur Archiv*, 55, pp. 176-185.

[7] Timoshenko, S., Young, D. H., and Weaver, W. Jr., 1974, *Vibration Problems in Engineering*, 4th Ed., Wiley, New York, N.Y.

[8] Veletsos, A. S., and Huang, T., 1970, "Analysis of Dynamic Response of Highway Bridges," *ASCE Journal of Engineering Mechanics Division*, 96, No. EM5, pp. 593-620.

[9] Yang, Y. B., and Lin, B. H., 1995, "Vehicle-bridge Interaction Analysis by Dynamic Condensation Method," *ASCE Journal of Structural Engineering*, 121, No. 11, pp. 1636-1643.

[10] Pesterev, A. V., and Bergman, L. A., 1997, "Response of Elastic Continuum Carrying Moving Linear Oscillator," *ASCE Journal of Engineering Mechanics*, 123, No. 8, pp. 878-884.

[11] Pesterev, A. V., and Bergman, L. A, 1998, "Response of Nonconservative Continuous System to a Moving Concentrated Load," *ASME Journal of Applied Mechanics*, 65, pp. 436-444.

[12] Omenzetter, P., and Fujino, Y., 2001, "Interaction of Non-conservative 1D Continuum and Moving MDOF Oscillator," *ASCE Journal of Engineering Mechanics*, 127, No. 11, pp. 1082-1088.

[13] Pesterev, A. V., and Tavrizov, G. A., 1994, "Vibrations of Beams with Oscillators. I: Structural Analysis Method for Solving the Spectral Problem," *Journal of Sound and Vibration*, 170, No. 4, pp. 521-536.

[14] Yang, B., 1996, "Integral Formulas for Non-self-adjoint Distributed Dynamic Systems," *AIAA Journal*, 34, No. 10, pp. 2132-2139.

[15] Pesterev, A. V., and Tavrizov, G. A., 1994, "On Inversion of Some Meromorphic Matrices," *Linear Algebra and Its Applications*, 212/213, pp. 505-521.

[16] Caughey, T. H., and O'Kelly, M. E., 1965, "Classical Normal Modes in Damped Linear Dynamic Systems," *Journal of Applied Mechanics*, ASME, 32, pp. 583-588.

[17] Meirovitch, L., 1967, *Analytical Methods in Vibrations*, The Macmillan Company, New York, N.Y.

[18] Daniels, R. W., 1978, *An Introduction to Numerical Methods and Optimization Techniques*, Elsevier North Holland, New York, N.Y.

[19] Thambiratnam, D., and Zhuge, Y., 1996, "Dynamic Analysis of Beams on an Elastic Foundation Subjected to Moving Loads," *Journal of Sound and Vibration*, 198, No. 2, pp. 149-169.

[20] Muscolino, G., and Palmeri, A., 2007, "Response of Beams Resting on Viscoelastically Damped Foundation to Moving Oscillators," *International Journal of Solids and Structures*, 44, pp. 1317-1336.

Table 1. Lowest 10 undamped natural frequencies (f) and damping ratios (ξ) for Euler-Bernoulli beam on viscoelastic foundation in Example 2.

Mode No.	Case 1 (a=L/12)		Case 2 (a=L/6)		Case 3 (a=L/4)	
	f (Hz)	ξ (%)	f (Hz)	ξ (%)	f (Hz)	ξ (%)
1	33.1	10.0	33.5	10.1	33.9	10.0
2	33.3	10.2	34.0	10.1	35.5	10.5
3	36.5	10.5	38.6	11.4	39.2	11.7
4	38.7	8.9	39.7	9.3	41.0	10.1
5	46.1	8.0	46.9	8.3	47. 7	8.6
6	55.9	6.2	56.6	6.6	57.1	6.8
7	69.8	5.1	70.4	5.4	70.9	5.7
8	86.6	4.0	87.0	4.3	87. 4	4.5
9	106.6	3.3	107.0	3.5	107.2	3.7
10	129.2	2.7	129.5	2.7	129.7	3.0

Table 2. Convergence of lowest 10 eigenvalues for Galerkin method in Example 2, Case 1 (a=L/12).

N_G	Error (%)									
	Mode No.									
	1	2	3	4	5	6	7	8	9	10
3	4.12	-	-	-	-	-	-	-	-	-
4	-	0.06	-	-	-	-	-	-	-	-
5	0.03	-	0.92	-	-	-	-	-	-	-
6	-	0.02	-	0.06	-	-	-	-	-	-
7	0.00	-	0.08	-	0.06	-	-	-	-	-
8	-	0.01	-	0.02	-	0.02	-	-	-	-
9	0.00	-	0.01	-	0.01	-	0.01	-	-	-
10	-	0.00	-	0.01	-	0.01	-	0.01	-	-
11	0.00	-	0.00	-	0.00	-	0.00	-	0.00	-
12	-	0.00	-	0.00	-	0.00	-	0.00	-	0.00

Table 3. Convergence of lowest 10 eigenvectors for Galerkin method in Example 2, Case 1 (a=L/12).

N_G	Error (%)									
	Mode No.									
	1	2	3	4	5	6	7	8	9	10
3	62.37	-	-	-	-	-	-	-	-	-
4	-	5.68	-	-	-	-	-	-	-	-
5	3.21	-	17.65	-	-	-	-	-	-	-
6	-	1.30	-	3.41	-	-	-	-	-	-
7	0.50	-	2.51	-	3.10	-	-	-	-	-
8	-	0.43	-	0.96	-	1.87	-	-	-	-
9	0.077	-	0.51	-	0.62	-	0.91	-	-	-
10	-	0.16	-	0.35	-	0.56	-	1.02	-	-
11	0.01	-	0.08	-	0.15	-	0.25	-	0.53	-
12	-	0.06	-	0.13	-	0.20	-	0.30	-	0.56

Table 4. Convergence of maximum mid-span beam deflection with increasing number of modes N_c in Example 2, Case 1 (a=L/12).

N_c	1	2	3	4	5	6	7	8	9	10
Max. $u_c(0.5L,t)$ (m)	0.0018	0.0022	0.0099	0.0093	0.0121	0.0121	0.0128	0.0128	0.0130	0.0131
Error (%)	-	20.88	77.44	-5.73	22.74	-0.30	5.90	0.17	1.52	0.15

Figure captions

Fig. 1. Interaction of 1D continuum and moving MDOF oscillator.

Fig. 2. Four-degree-of-freedom vehicle model in Examples 1 and 2.

Fig. 3. Mid-span deflection of the beam in Example 1.

Fig. 4. Vehicle body displacement in Example 1.

Fig. 5. Euler-Bernoulli beam on viscoelastic foundation in Example 2.

Fig. 6. Real part of the first three continuum right mode shapes in Example 2.

Fig. 7. Imaginary part of the first three continuum right mode shapes in Example 2.

Fig. 8. Time histories of mid-span deflection for different number of modes in Example 2, Case 1 ($a=L/12$).

Fig. 9. Time history of real part of modal coordinates for the first three modes in Example 2.

Fig. 10. Time history of imaginary part of modal coordinates for the first three modes in Example 2.

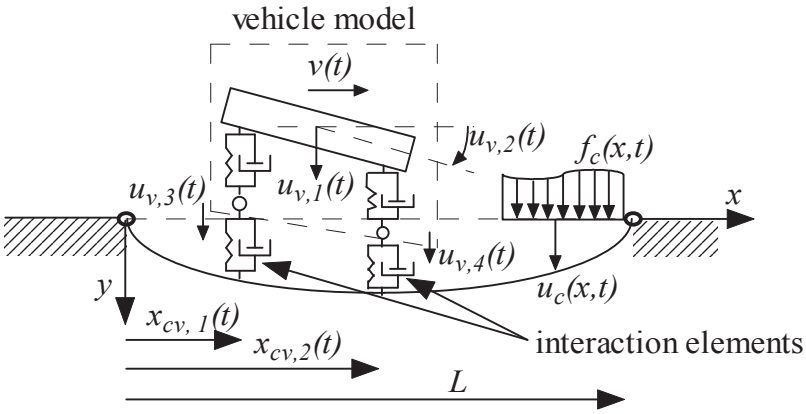

Fig. 1 Interaction of 1D continuum and moving MDOF oscillator.

Omenzetter

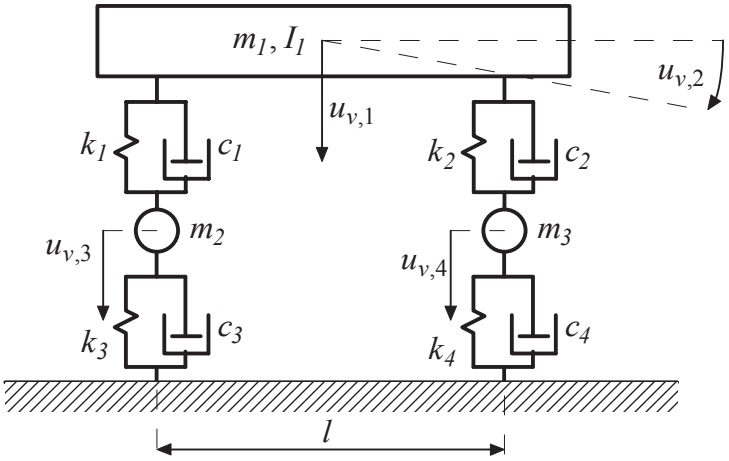

Fig. 2 Four-degree-of-freedom vehicle model.

Omenzetter

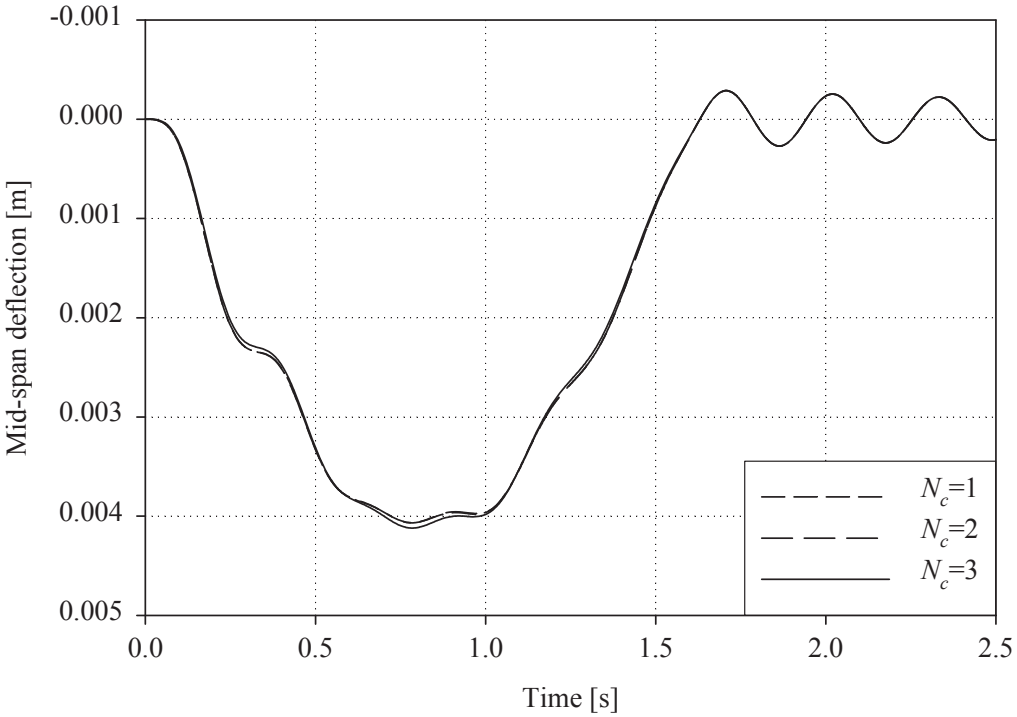

Fig. 3. Mid-span deflection of the beam.

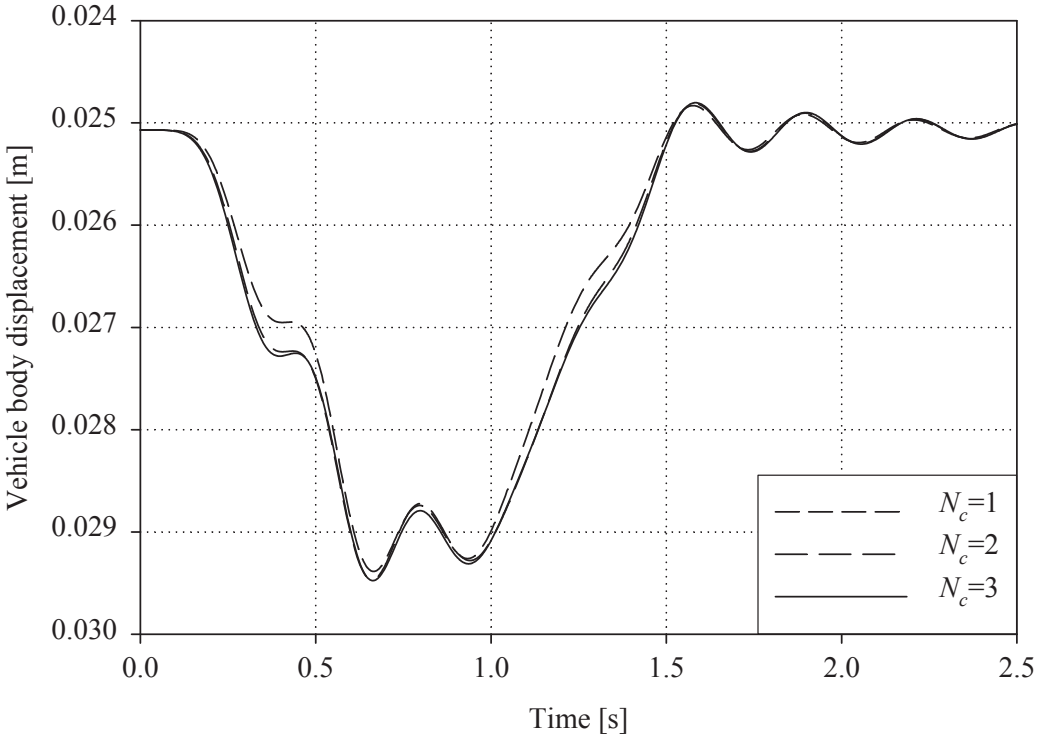

Fig. 4. Vehicle body displacement.

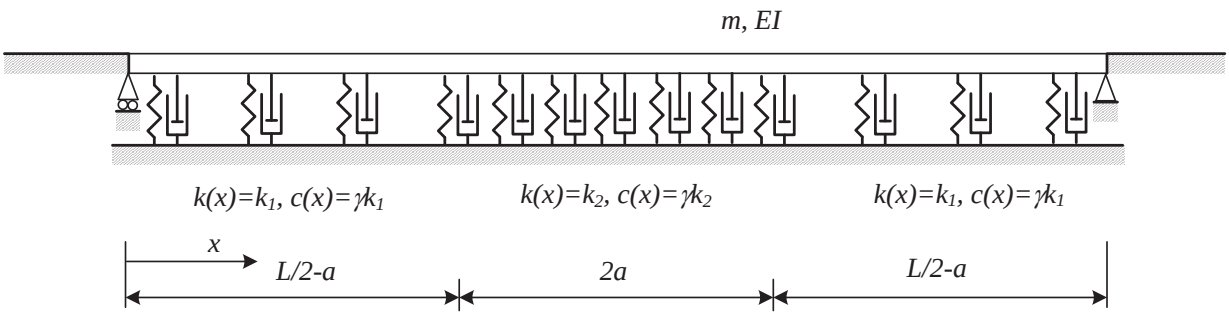

Fig. 5. Euler-Bernoulli beam on viscoelastic foundation in Example 2.

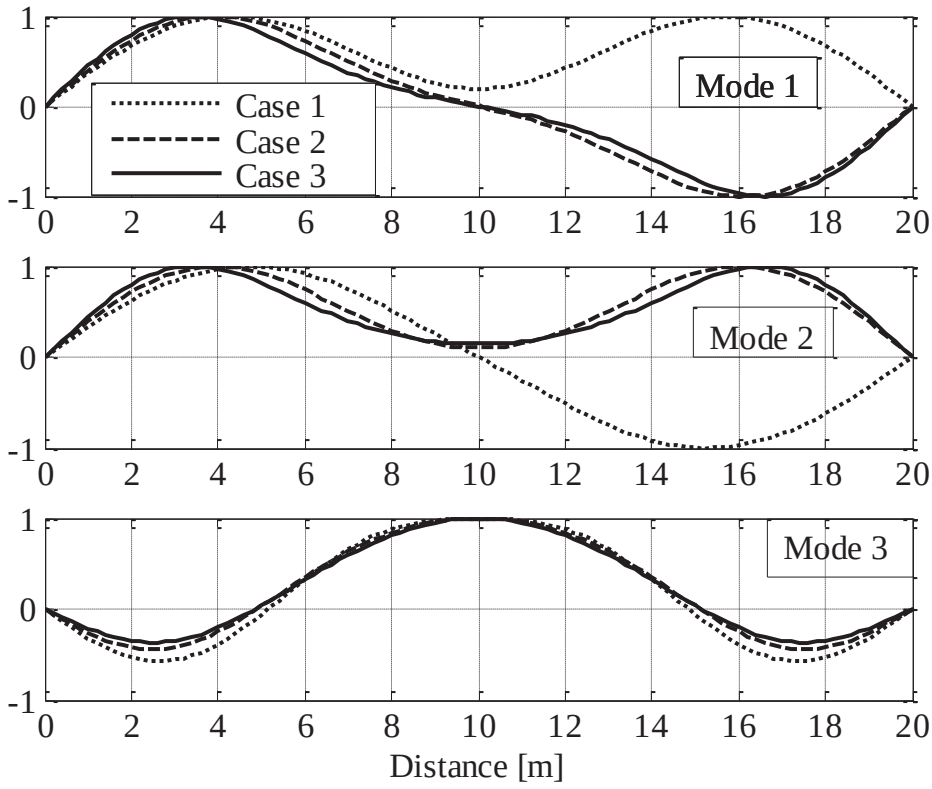

Fig. 6. Real part of the first three continuum right mode shapes in Example 2.

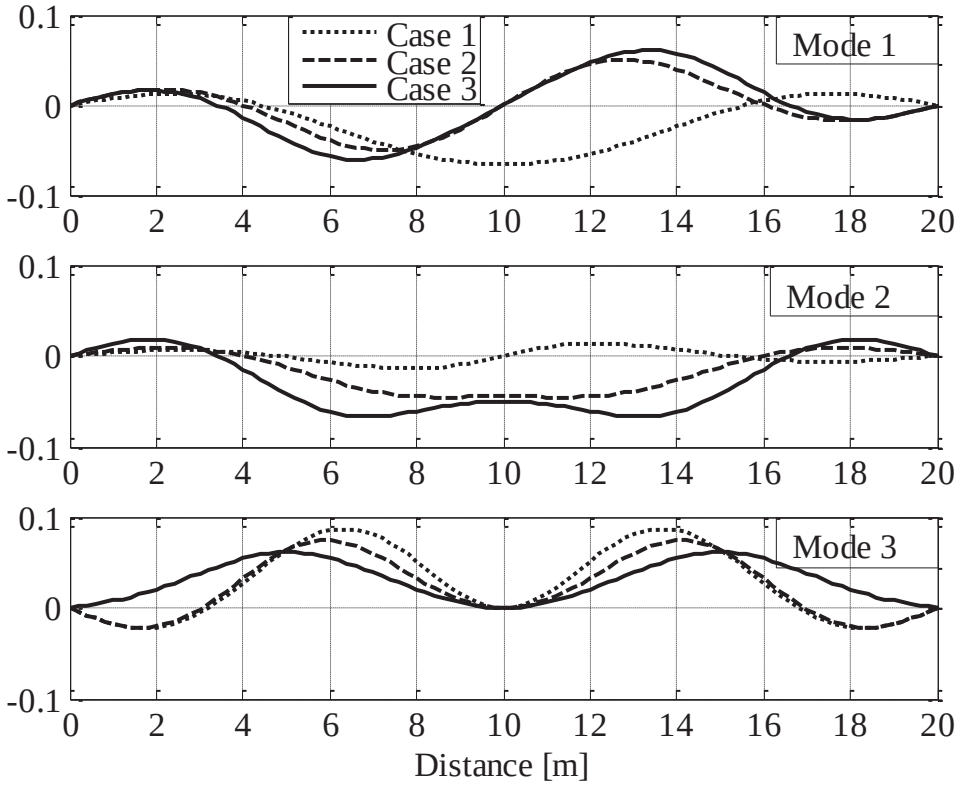

Fig. 7. Imaginary part of the first three continuum right mode shapes in Example 2.

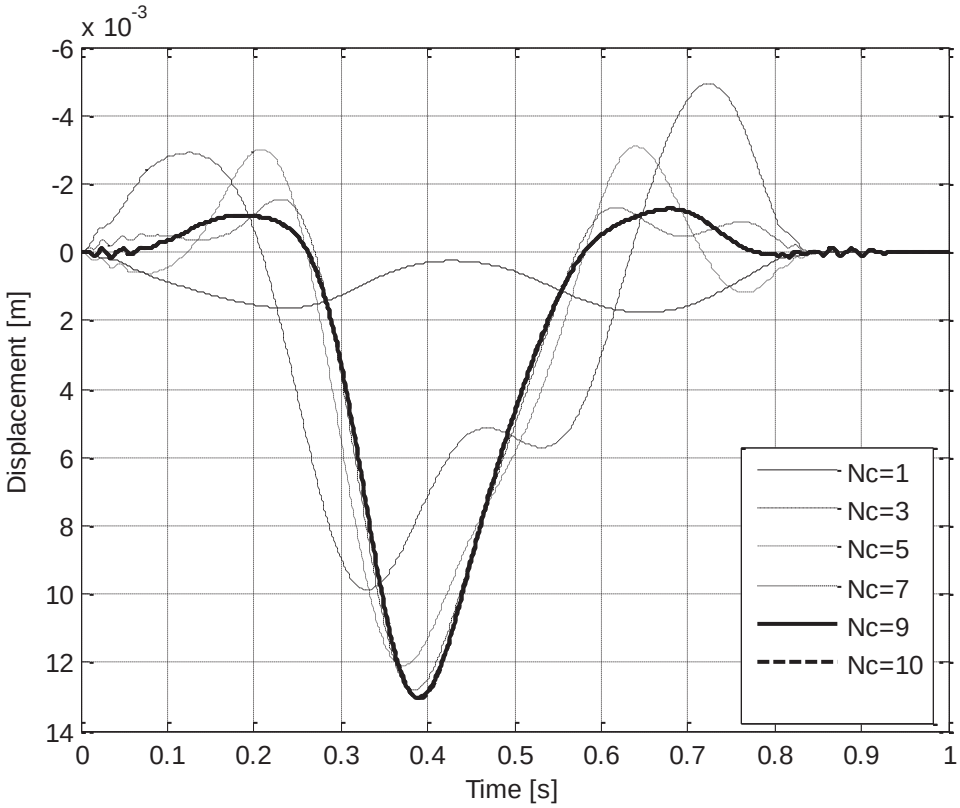

Fig. 8. Time histories of mid-span deflection for different number of modes in Example 2, Case 1 (a=L/12).

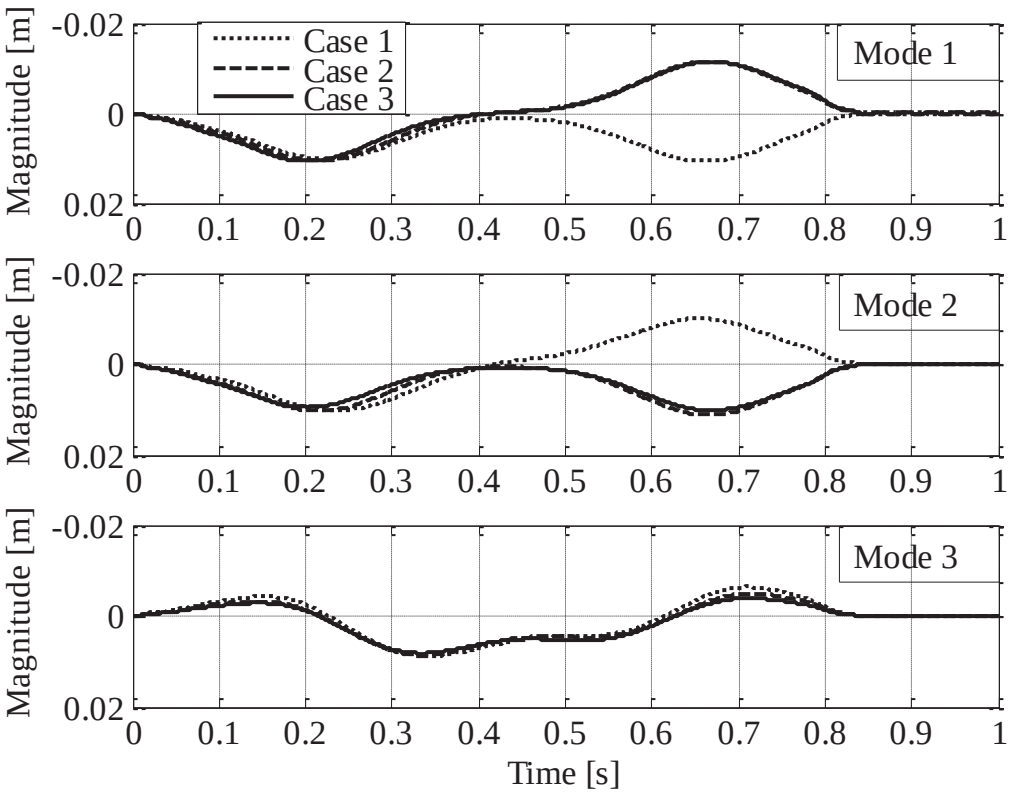

Fig. 9. Time history of real part of modal coordinates for the first three modes in Example 2.

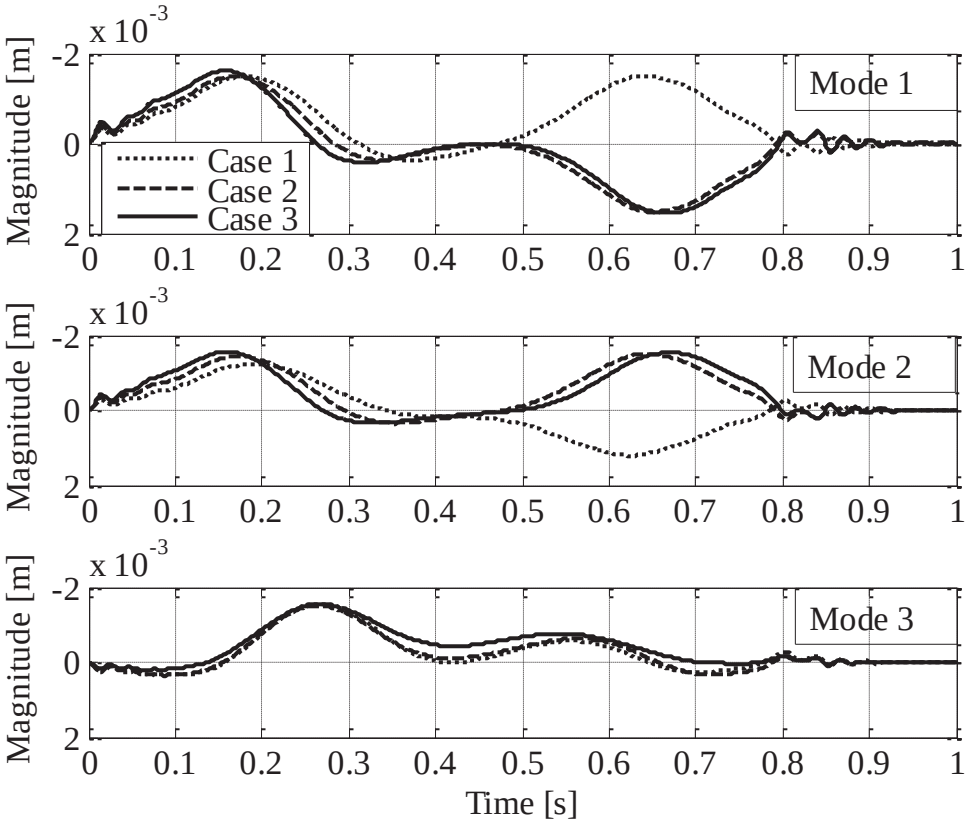

Fig. 10. Time history of imaginary part of modal coordinates for the first three modes in Example 2.